X-ray Microbeam Diffraction Measurements in Polycrystalline Aluminum and Copper Thin Films

L. E. Moyer[1], G. S. Cargill III[1], W. Yang[2], B. C. Larson[2], G. E. Ice[2]
[1] Dept. Mat. Sci. and Engr., Lehigh University, Bethlehem, PA 18015, USA
[2] Solid State Div., Oak Ridge National Lab., Oak Ridge, TN 37831, USA

ABSTRACT

Thermally induced residual strains in polycrystalline Cu and Al films on single crystal Si and glass substrates, respectively, have been examined on a grain-by-grain basis by x-ray microbeam diffraction. The crystallographic orientation and the deviatoric strain tensor, ε_{ij}^*, are determined for each grain by white beam Laue diffraction. From grain orientation mapping and strain tensor measurements, information is obtained about the distributions of strains for similarly oriented grains, about strain variations within single grains, and about grain-to-grain correlations of strains. This type of information may be useful in developing and testing theories for intergrain effects in strain evolution in polycrystals.

INTRODUCTION

Integrated circuit devices are typically connected by patterned lines of a passivated polycrystalline metal, usually copper or aluminum. As devices and interconnects continue to decrease in size, electrical performance and mechanical reliability become greater concerns. Thermal strains develop in interconnects during fabrication and during operation at elevated temperatures due to the difference in thermal expansion between interconnects and surrounding layers. These strains can lead to failures from voids and hillocks in interconnects. X-ray diffraction is a well-established technique for measuring average elastic strains in polycrystalline materials. Recent advances in third generation synchrotron sources and focusing optics now provide the means for grain-by-grain x-ray measurements [1-5]. X-ray microbeam strain measurements on polycrystalline Cu and Al films are described in this paper.

EXPERIMENT

The microdiffraction experiments were performed at the Advanced Photon Source, Argonne National Lab, on the UNICAT beamline. A schematic of the setup is shown in Fig.1. Kirkpatrick-Baez (K-B) focusing mirrors are used to obtain a sub-micron x-ray beam for microdiffraction. The sample is positioned on a translation stage at an angle of 45° from the incoming beam. A CCD detector located directly above the sample records the Laue diffraction pattern. A computer program developed at Oak Ridge National Lab [2] calculates the orientation matrix of each grain in the Laue pattern. The program also measures the deviations of the Laue

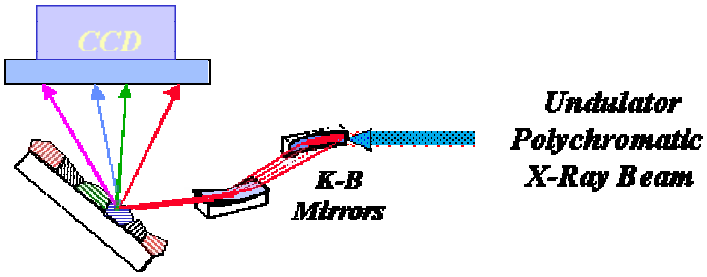

Figure 1. Schematic of setup for microbeam x-ray diffraction experiments (*from B. C. Larson et al., UNICAT and ORNL).*

spots from the unstrained positions to obtain a complete deviatoric strain tensor.

A 1 μm thick polycrystalline Cu film with a (111) fiber texture on a (001) oriented single crystal Si substrate was investigated. The sample was heated to 400°C, held for 1 hour, and then was cooled to room temperature. Microdiffraction measurements were then made at room temperature. A 2 μm thick polycrystalline Al film with a (111) fiber texture on a glass substrate was also investigated. The sample was heated from room temperature to 300°C for in-situ x-ray microdiffraction measurements during two thermal cycles.

RESULTS

X-ray microbeam diffraction measurements at room temperature were made after the heat treatment for the Cu sample. Similar experiments have been reported by Chung et al. [3] and Tamura et al. [5]. The crystallographic orientation and the deviatoric strain tensor, ε_{ij}^*, defined in Eq. (1), were determined for each grain.

$$\varepsilon^*_{ij} = \begin{pmatrix} \varepsilon^*_{11} & \varepsilon^*_{12} & \varepsilon^*_{13} \\ \varepsilon^*_{12} & \varepsilon^*_{22} & \varepsilon^*_{23} \\ \varepsilon^*_{13} & \varepsilon^*_{23} & \varepsilon^*_{33} \end{pmatrix} = \begin{pmatrix} \varepsilon_{11} - \frac{\Delta}{3} & \varepsilon_{12} & \varepsilon_{13} \\ \varepsilon_{12} & \varepsilon_{22} - \frac{\Delta}{3} & \varepsilon_{23} \\ \varepsilon_{13} & \varepsilon_{23} & \varepsilon_{33} - \frac{\Delta}{3} \end{pmatrix} \tag{1}$$

In Eq. (1) $\Delta = \varepsilon_{11} + \varepsilon_{22} + \varepsilon_{33}$, and the sum of the diagonal terms in the deviatoric tensor is zero,

$$\varepsilon^*_{11} + \varepsilon^*_{22} + \varepsilon^*_{33} = 0. \tag{2}$$

The average grain size for the Cu sample was approximately 1 μm, although some grains were larger. A grain orientation map for this sample is shown in Fig. 2. Each of the small squares in Fig. 2 is 0.5 μm x 0.5 μm and the entire mapped area is 2.5 μm x 7 μm. Boundaries within individual squares are drawn to indicate which grains were present, although the exact locations of the boundaries were not determined. Table I shows the average deviatoric perpendicular strains for all grains, (111) oriented grains, (110) oriented grains, and (100) oriented grains. Root-mean-squared strain deviations are also shown. The average deviatoric perpendicular strains are similar for the different orientations, except in the case of (100) grains where the average strain is more compressive than the others. Vinci et al. [6] have reported residual thermal strains in (100) grains to be 50% larger than those in (111) grains in Cu thin films, which they attribute to the larger in-plane stiffness of (111) grains.

Strain mapping of the perpendicular deviatoric strain ε^*_{33} for the area in Fig. 2 is shown in

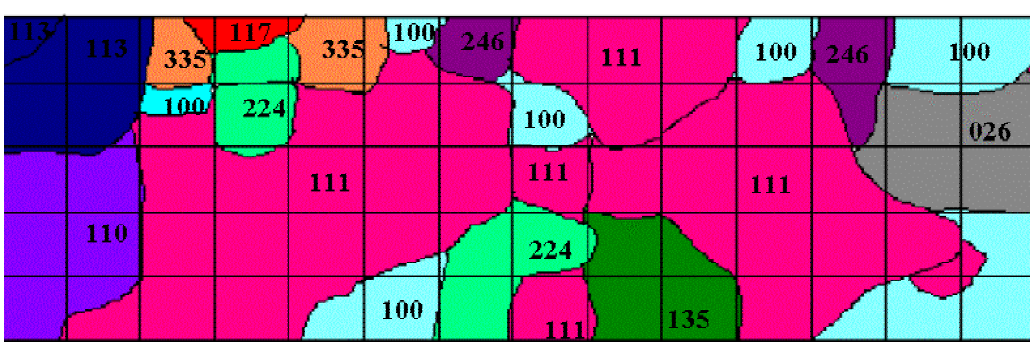

Figure 2. Grain orientation map for 1 μm thick Cu sample.

Table I. Average deviatoric perpendicular strains and RMS deviation of strains for different Cu grain orientations.

Orientation	$<\varepsilon^*_{33}>$	RMS deviation
All	-0.0026	0.0009
111	-0.0024	0.0008
110	-0.0024	0.0004
100	-0.0034	0.0009

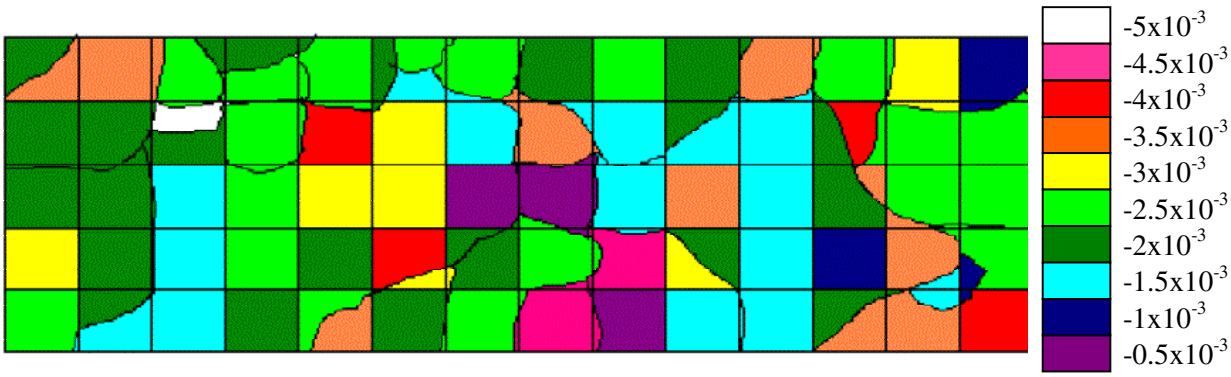

Figure 3. Strain map for 1 μm thick Cu sample.

Fig. 3. Not only are there large variations in strain over the region of the sample shown, there are also large strain variations within single grains. For many grains shown, the strain changes are more apparent near the grain boundaries, which may be due to in-plane strain differences between adjacent grains of different orientations.

For the Al sample, two thermal cycles were performed from room temperature to 300° C and back to room temperature. Heating and cooling times and temperatures are shown in Fig. 4. Measurements were made at room temperature, during heating, at 300°C, and during cooling. For both cycles the sample was held at 300°C for six hours or more, which was long enough for the average strains to relax. Deviatoric strains were measured during both thermal cycles. Calculations of deviatoric perpendicular strain using differential thermal expansion but without relaxation are shown in Fig. 5 together with experimental data for the two cycles. In Fig. 5 the experimental data are color-coded to indicate the grain orientations for each data point. Negative strain values are compressive and positive strain values are tensile. No clear trend is seen of different behavior for differently oriented grains.

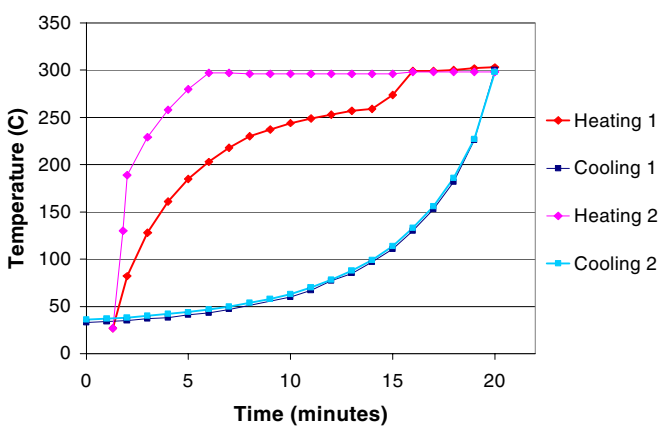

Figure 4 Temperatures and time for thermal cycles.

Thouless et al. [7] developed equations to describe stress development and relaxation in films during thermal cycling based on the deformation mechanism maps of Frost and Ashby [8]. Thouless et al. [7] and Vinci et al. [6] used these equations to model thin film behavior during

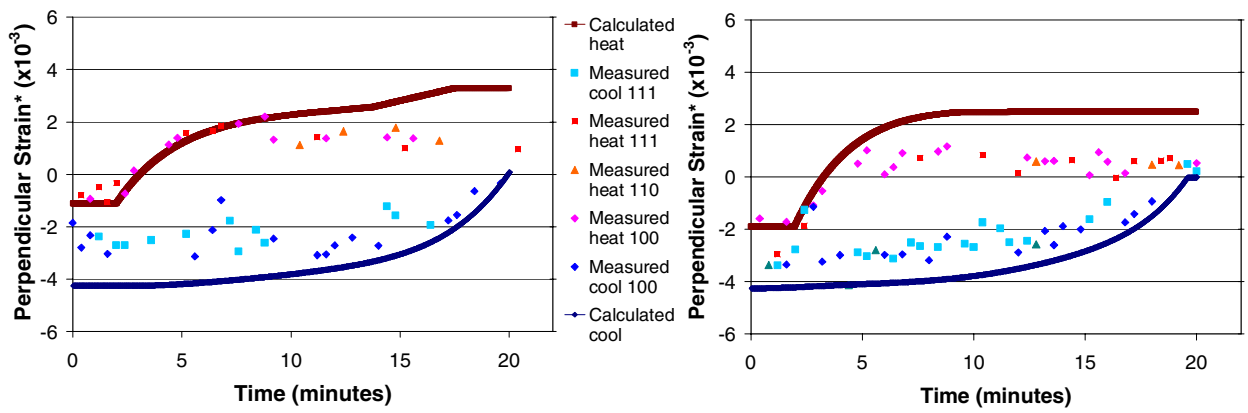

Figure 5 Perpendicular deviatoric strain vs. time for first (left) and second (right) thermal cycles for Al sample. Calculated curves do not include relaxation.

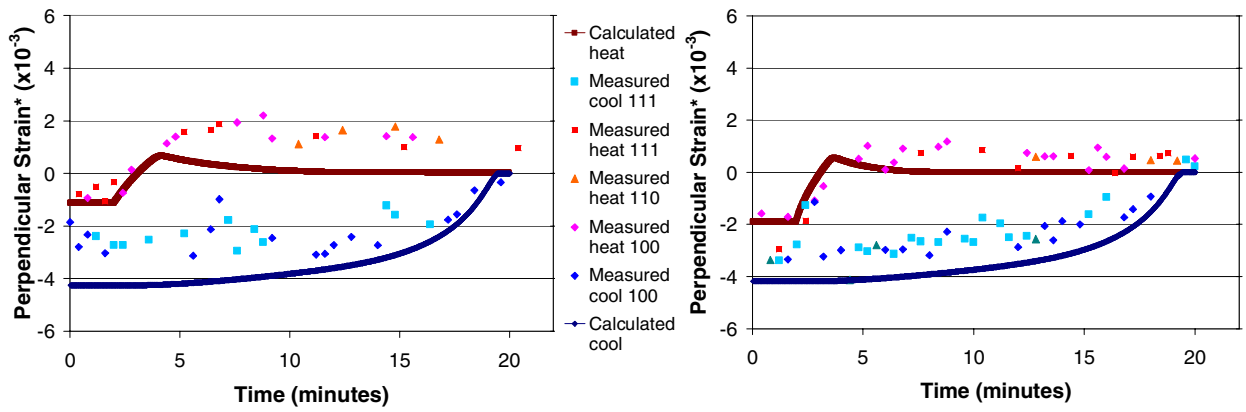

Figure 6. Perpendicular deviatoric strain vs. time for first (left) and second (right) thermal cycles for Al sample. Calculated curves include relaxation.

thermal cycling. We have also used these equations and material parameters from Frost and Ashby [8] for bulk Al to model our film behavior. The calculated curves are shown in Fig. 6 along with experimental data.

The calculated heating curves for both thermal cycles match experimental data initially when relaxation is not included, as shown in Fig. 5. The measured strains are lower than the calculated curves without relaxation after this initial agreement, indicating that relaxation occurs in the sample. The calculated strains including relaxation, shown in Fig. 6, also agree with the experimental data initially, but they are lower than the experimental data after this initial agreement, which indicates that the sample is not relaxing as much as the model calculations predict. Calculated cooling curves without relaxation for both thermal cycles show that relaxation occurs in the sample. When relaxation is included in the calculation for cooling there is very little change compared with the calculation without relaxation, because of the rapid initial cooling rate. During cooling the sample relaxes more than predicted by the model calculations.

Grain orientation mapping from area scans taken at room temperature before and after the first thermal cycle are shown in Figs. 7(a) and (b). The areas are different due to uncontrolled sample movement during heating and cooling. The hexagon in Fig. 7(c) shows the colors used to represent different grain orientations. Black indicates areas that did not index. The average deviatoric perpendicular strain for all grains, (111) grains, (110) grains, and (100) grains for each area are shown in Table II along with root-mean-squared strain deviations. The average

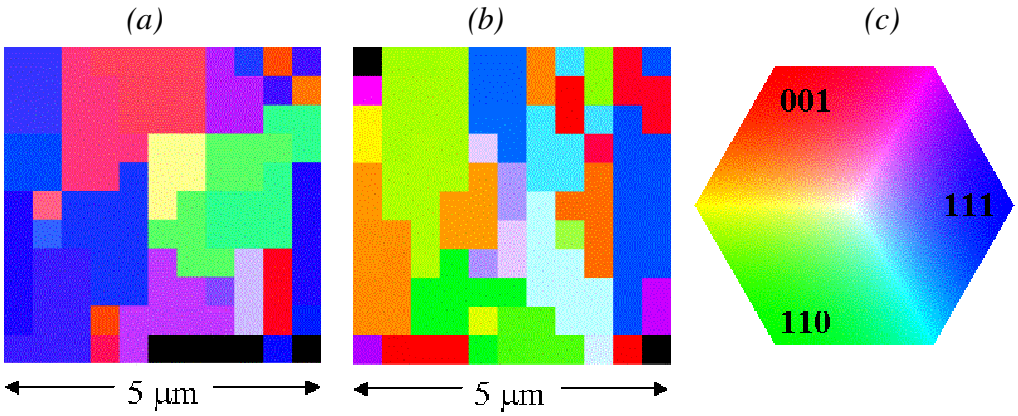

Figure 7. (a) Orientation map of Al sample before thermal cycle. (b) Orientation map of different area (see text) of Al sample after thermal cycle. (c) Orientation legend.

Table II. Average deviatoric perpendicular strains and RMS deviations of strains for different Al grain orientations before and after first thermal cycle.

Orientation	$\langle\varepsilon^*_{33}\rangle$ before thermal cycle (as in Fig.7(a))	RMS deviation	$\langle\varepsilon^*_{33}\rangle$ after thermal cycle (as inFig.7(b))	RMS deviation
All	-0.0013	0.0004	-0.0016	0.0006
111	-0.0013	0.0005	-0.0016	0.0005
110	-0.0015	0.0001	-0.0018	0.0005
100	-0.0013	0.0003	-0.0015	0.0008

deviatoric perpendicular strains are nearly the same for all orientations, which may be due to the fact that Al is nearly isotropic elastically, except perhaps for slightly larger values of $\langle\varepsilon^*_{33}\rangle$ for (110) grains. Perpendicular deviatoric strain maps for the areas in Figs. 7(a) and (b) are shown in Figs. 8(a) and (b).

Red areas in Fig. 8 are regions with $\varepsilon_\perp^* < 0$, which have higher compressive deviatoric perpendicular strain as expected at room temperature. The blue areas are regions of the sample with $\varepsilon_\perp^* \approx 0$, or in some cases $\varepsilon_\perp^* \geq 0$. Black indicates areas that did not index. A wide range of deviatoric strains exists in the sample. Also, some grains have nearly the same strain throughout their area, while others have large strain gradients from one part of the grain to another. Spolenak et al. [4] have reported deviatoric stress maps for a polycrystalline Al 0.5 wt.% Cu film several weeks after cooling from its 400°C deposition temperature, and observed that the stress state within one grain can be strongly influenced by its neighbors.

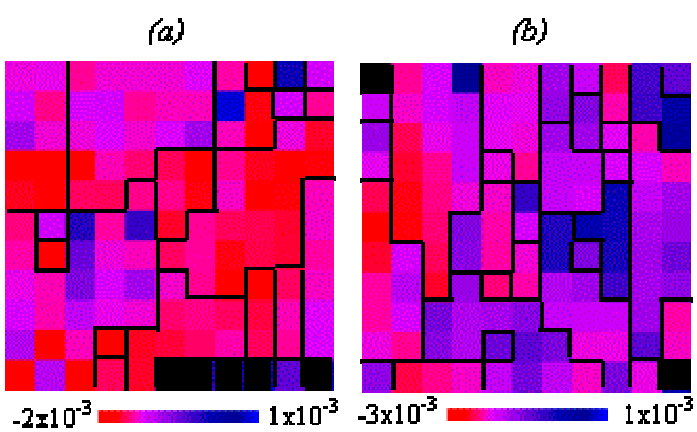

Figure 8. (a) Strain map for area shown in Fig. 7(a). (b) Strain map for area shown in Fig. 7(b).

CONCLUSIONS

From the Cu orientation and strain maps, it is clear that large strain gradients exist not only in the film in general but within some single grains. For many grains shown, the strain changes are more apparent near the grain boundaries, perhaps due to in-plane strain differences between adjacent grains of different orientations. The average deviatoric perpendicular strains in the Cu film are similar for the different orientations, except for (100) grains where the average strain is more compressive for (100) than the other grain orientations.

Figs. 5 and 6 clearly show that relaxation is important for the Al sample. During heating, the sample is not relaxing as much as the calculations with bulk material parameters predict. During cooling the sample is relaxing more than the calculations predict. Average deviatoric perpendicular strains do not seem to depend on grain orientation, possibly due to Al being nearly isotropic elastically, except for the slightly larger $<\varepsilon^*_{33}>$ for (110) grains. Grain orientation maps and strain maps of the Al sample before and after thermal cycling reveal possible correlations between strain and orientation.

ACKNOWLEDGMENTS

This research was supported in part by NSF grants DMR-9796284 and DMR-0312189 at Lehigh University and by the SURA/ORNL Summer Cooperative Research Program. ORNL research was sponsored by the US Department of Energy, Office of Basic Energy Sciences, Division of Materials Sciences under Contract No. DEAC05-00OR22725 with Oak Ridge National Laboratory, managed by UT-Battelle, LL. Work performed on the UNICAT beamline at the APS was supported in part by DOE Grant No. DE-FG02-99ER45743; UNICAT is operated by UIUC, ORNL, NIST, and UOP Research, Inc. The operation of the APS is sponsored by the DOE. We also thank the SURA and UNICAT staff members for support and guidance.

REFERENCES

1. G.S. Cargill, III, L. Moyer, W. Yang, B.C. Larson and G.E. Ice, *Mater. Sci. Forum* **426-432**, 3945 (2003).
2. J.S. Chung and G.E. Ice, *J. Appl. Phys.* **86**, 5249 (1999).
3. J.S. Chung, N. Tamura, G.E. Ice, B.C. Larson and J.D. Budai, *Mater. Res. Soc. Proc.* **563**, 169 (1999).
4. R. Spolenak, W.L. Brown, N. Tamura, A.A. MacDowell, R.S. Celestre, H.A. Padmore, B. Valek, J.C. Bravman, T. Marieb, H. Fujimoto, B.W. Batterman, and J.R. Patel, *Phys. Rev. Lett.* **90**, 096102 (2003).
5. N. Tamura, A.A. MacDowell, R.S. Celestre, H.A. Padmore, B. Valek, J.C. Bravman, R. Spolenak, W.L. Brown, T. Marieb, H. Fujimoto, B.W. Batterman, and J.R. Patel, *Appl. Phys. Lett.* **80**, 3724 (2002).
6. R.P. Vinci, E.M. Zielinski and J.C. Bravman, *Thin Solid Films* **262**, 142 (1995).
7. M.D. Thouless, J. Gupta and J.M.E. Harper, *J. Mater. Res.* **8**, 1845 (1993).
8. H.J. Frost and M.F. Ashby, *Deformation-Mechanism Maps: The Plasticity and Creep of Metals and Ceramics* (Pergamon Press, 1982).